(Received 3 July 2024, Accepted 12 August 2024, Scheduled 24 August 2024)

Compact Wideband Wide-Beam Circularly Polarized Loop Antenna Using Sequential Rotation Feeding Technology

Sihan Liu, Hongmei Liu*, Youjie Zeng, Yanjie Pei, and Zhongbao Wang

School of Information Science and Technology, Dalian Maritime University, Dalian, Liaoning 116026, China

ABSTRACT: In this paper, a wideband wide-beam circularly polarized (CP) antenna excited by sequential rotation feeding technology is proposed. The antenna is primarily constituted of a loop radiating element and a reactive impedance structure (RIS) cavity. The loop radiator is stimulated by a curved feeding line through six slots etched on the ground, thereby enabling the antenna to achieve broadband performance. In order to achieve a wide 3-dB axial-ratio beamwidth (ARBW), as well as exhibit less effect on the half-power beamwidth (HPBW), a RIS cavity is introduced beneath the loop radiator. To validate the proposed structure, a prototype was constructed and subjected to a series of tests. The results indicate that the bandwidth of the antenna is 187.5% (0.11 $\sim$ 3.41 GHz) under a 10-dB return loss. In the frequency band spanning from 1.07 GHz to 2.1 GHz, the AR is less than 3 dB, yielding a bandwidth of 64.98%. Furthermore, at the frequencies of 1.2 GHz, 1.5 GHz, and 1.8 GHz, the proposed antenna demonstrates wide beam characteristics, with the HPBW exceeding 90°, and the 3-dB ARBW within 162° 224°. In addition, since no extra feeding network is utilized, the antenna is compact in size.

1. INTRODUCTION

In comparison to linearly polarized antennas, circularly polarized (CP) antennas have garnered significant interest due to the advantages of enhanced coverage, reduced polarization mismatch loss, and reduced multipath distortion [1]. Optimal CP antenna should exhibit the performances of compactness and wideband [2–5]. The current research trend is the investigation of wide-beam performance based on broadband performance [6, 7].

Generally, multi-feed point techniques are used to achieve wide impedance and axial ratio bandwidths, but mostly require feeding networks composed of couplers or power splitters, which results in large size, high loss, and complex topology [8, 9]. By utilizing sequential rotation feeding technology [10], this issue can be resolved. This can dispense with the couplers or power dividers that are typically required by a traditional feed network and achieve the requisite matching and shaft ratio performance through structural design [11–15]. The sequential rotary feed structure of [12] is still essentially a power distributor in design. In [14], the antenna requires two input ports to achieve the broadband of the sequential rotary feed structure.

Furthermore, in terms of performance, a wide-beam CP antenna can facilitate the transmission and reception of signals in a wide coverage. In order to maintain high polarization purity over a wide angular range, it is necessary to broaden the 3-dB axial ratio beamwidth (ARBW), where the effective methods are metasurface, short-circuit pin, and slotted ground [16, 17]. Besides, half-power beamwidth (HPBW) is also a performance index that cannot be overlooked. The coverage range of the antenna's HPBW should be guaranteed in order to enhance the effectiveness of low-altitude signal reception [18–21]. In [18] and [19], curved radiating arms and a corrugated back cavity are used, where the 3-dB ARBWs reach more than 200° with the HPBWs of larger than 100°. In [20], metallic cavity is applied to expand the 3-dB ARBW while maintaining a stable HPBW. In [21], the authors demonstrate the successful widening of the HPBW by loading the metal ring, as well as introducing slots on the waveguide. The overlapped beamwidth between 3-dB ARBW and HPBW reaches more than 130°. However, the aforementioned articles do not show the wideband characteristics, and only the features of wide 3-dB ARBW and HPBW are obtained.

To the authors' knowledge, only several literatures report the wideband CP antennas with wide beamwidth. In [22], by utilizing two inverted S-shaped curved arms, the 3-dB ARBW and HPBW of more than 100° and 84°, respectively, are achieved in the bandwidth of 42%. Nevertheless, the utilization of a balun has resulted in a certain degree of complexity in the feed, and the dimension is considerably large. In [23], orthogonal dipoles conformal to spherical shell substrate are studied, where a wide bandwidth of 55% is obtained, and the beamwidths are enlarged to around 100°. However, except that the beamwidth is not wide enough, the utilization of conformal technology and a four-feed network have resulted in an increase in the difficulty and cost of assembly. In [24], short vertical plates are introduced to balance the current between the dipole and the slot ground, which ultimately achieves the 3-dB ARBW of 100° and HPBW of 120° while exhibiting a wideband exceeding 70%. In common with [23], since the vertical metallic plate is included, the assembly difficulty is increased. Besides, the location error

* Corresponding author: Hongmei Liu (lhm323@dlmu.edu.cn).

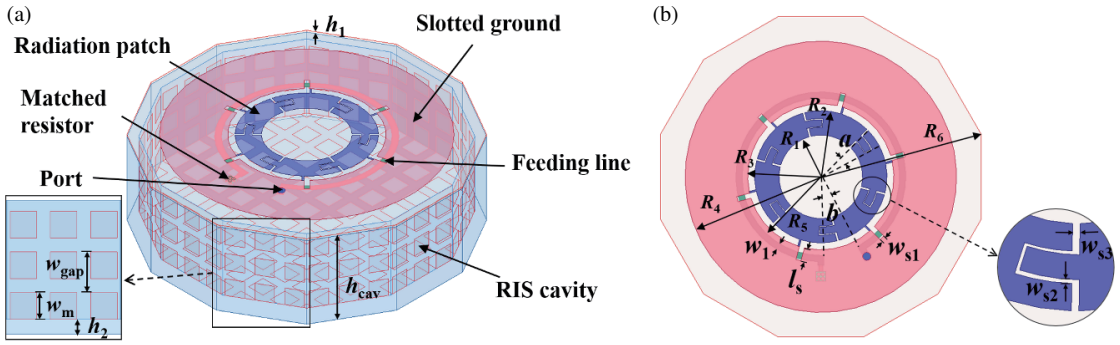

FIGURE 1. Configuration of the proposed antenna. (a) 3-D view. (b) Top view of radiant part.

of the vertical metallic plate may worsen the antenna performances. Thus, it is still a challenge to design a wideband CP antenna with wide beam and compact structure.

In the paper, a compact CP antenna with wideband and wide beamwidth is proposed based on the sequential rotation feeding technology. It is noteworthy that by setting the feeding line through the equally spaced ground slots, requisite phase shift for the antenna can be provided, and ultimately the impedance matching and AR bandwidths of 187.5% and 64.98% are achieved, respectively. Furthermore, following the introduction of the RIS cavity, the antenna exhibits 3-dB ARBWs of greater than 162° and HPBWs of at least 90°. The size is only $0.33\lambda_0 \times 0.33\lambda_0 \times 0.10\lambda_0$. The aforementioned antenna is characterized by a wide bandwidth and commendable beamwidth performance, which are achieved under the premise of single feed and compact size. It demonstrates considerable potential in satellite navigation and positioning applications.

2. ANTENNA CONFIGURATION AND DESIGN PROCEDURE

2.1. Configuration of the Proposed Antenna

Figure 1 illustrates the configuration of the proposed CP antenna, which encompasses a loop radiator and a reactive impedance structure (RIS) cavity. The loop radiator consists of a loop radiation patch, a slotted ground, and an arc microstrip feeding line, which are etched on a thin substrate of F4B ($\varepsilon_r = 2.2$, $\tan\delta = 0.02$, $h_1 = 0.6$ mm). The loop radiation patch has six staggered coupled slots at an angle of a. The slotted ground is positioned around the patch. Beneath the slots, a curved feeding line is etched to excite the radiation patch. The six slots with size of $l_s \times w_{s1}$ are arranged at equal intervals on the ground, ensuring that the feeding line can provide a suitable phase-shift to produce CP wave. This coupled feed structure is designated as traveling wave feed, where two ends of the curved feeding line are connected to the 50-Ω resistor and the input port, respectively. In accordance with the transmission line theory, the operational state of the feeding line can be modified by adjusting the radius R_5, width w_1, and length (adjust angle b) of the feed line, thus enabling it to reach the travelling wave state and facilitating the matching of the antenna. The sequential rotation feeding technique described in this paper necessitates that the mth patch undergoes both a physical rotation of φ_{pm} and a feed phase shift of φ_{em}. The expressions of φ_{pm} and φ_{em} are shown below:

$$\varphi_{em} = (m-1)\frac{P\pi}{M} \tag{1a}$$

$$\varphi_{pm} = (m-1)\frac{P\pi}{M} \quad (1 \le m \le M) \tag{1b}$$

where M is the number of equivalent radiation elements, and P is the number of sequential rotations. The length of the feed line situated beneath the adjacent slot has been determined to be about $\lambda_g/6$ (λ_g is 1.5 GHz), which has the effect of producing an appropriate 60° phase shift between the two adjacent slots for the transmission. The travelling wave feeding mode with sequential rotating feed excitation enables the antenna to achieve stable wide matching bandwidth and wide CP bandwidth.

A RIS cavity is positioned beneath the thin substrate in order to reduce the backward radiation, extend the ARBW of the antenna, as well as exhibit less effect on the HPBW. The mechanism of action of the metal reflector is based on the principle that the field reflection of the reflector alters the phase response, thereby making the phase difference to approximately 90° over a broader angular range. The reflection phase can be modified by modifying the dimensions and spacing of the RIS unit, as well as the height between the RIS and the radiator. In particular, the RIS elements with a side length of w_m are uniformly distributed on the side wall and bottom plate of the cavity with a thickness of h_2 at w_{gap} intervals. It is noteworthy that the radius of the cavity is identical to that of the upper substrate, with both dimensions being R_6. In Subsection 3.2, the position parameters of the RIS cavity are subjected to a comprehensive analysis, and the impact of varying parameters on the antenna beamwidth is investigated. After optimization using the HFSS, final dimensions of the proposed antenna are shown in Table 1.

2.2. Evolution of the Antenna

This section presents the evolution of the proposed antenna, as illustrated in Figure 2. Figures 3 and 4 show the compared results, including $|S_{11}|$, AR, 3-dB ARBWs, and HPBW. It is noted that the beamwidth shown in Figure 4 is plotted at the center frequency of 1.5 GHz.

TABLE 1. Dimensions of the proposed antenna.

Parameters	h_1	h_2	h_{cav}	w_m	w_{gap}	R_1	R_2	R_3	R_4
Size (mm)	0.6	3	27	5.4	8.2	12	19	21	39
Parameters	R_5	R_6	w_1	a	b	l_s	w_{s1}	w_{s2}	w_{s3}
Size (mm)	22.58	47.62	1.84	17°	30°	3.8	1.5	0.3	0.6

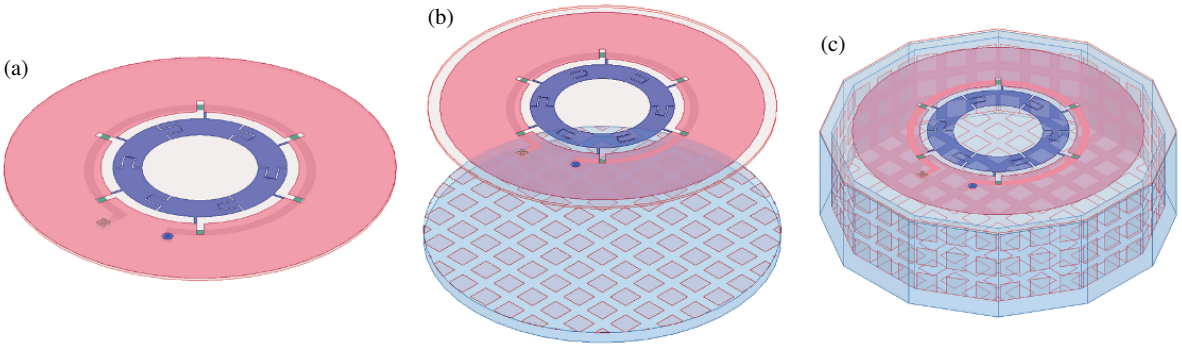

FIGURE 2. Evolutions of the proposed Wide-beamwidth loop antenna. (a) Ant. 1. (b) Ant. 2. (c) Ant. 3.

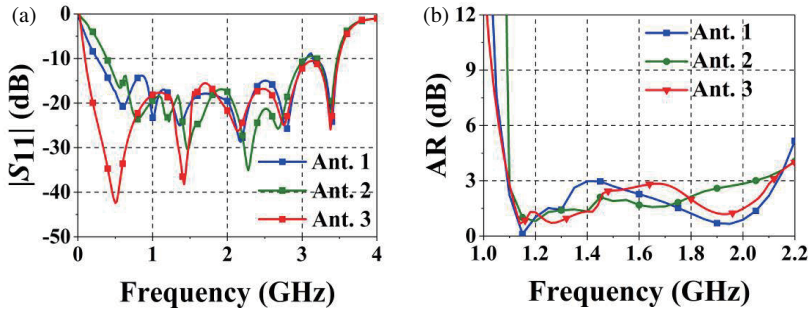

FIGURE 3. Simulated results of the three evolutions. (a) $|S_{11}|$. (b) AR.

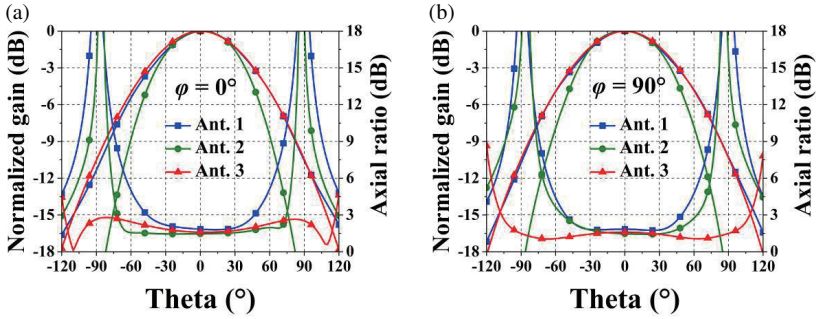

FIGURE 4. Simulated results of the three evolutions. (a) HPBWs and ARBWs at $\varphi = 0°$. (b) HPBWs and ARBWs at $\varphi = 90°$.

Firstly, a single-feed loop antenna with sequential rotation network is designed (named as Ant. 1), as shown in Figure 2(a). Here, an equally spaced curved slot is introduced into the traditional microstrip loop patch. This modification has the effect of reducing the circumference of the loop, which is beneficial for overall size miniaturization. The branch extending from the central portion of each pair of slots is linked to the ground slot, thus enabling the loop patch to receive the series coupling excitation resulting from the microstrip feeding line. The utilization of this sequential rotary feed technique ensures that the radiating element receives an accurate phase shift from the feed current, thereby guaranteeing CP performance. Figure 5 illustrates the surface current distribution on the loop patch of Ant. 1 at 1.5 GHz. A comparison of the current direction at 0, T/4, T/2, and 3T/4 reveals that the current rotates in a counterclockwise direction, thereby producing right-handed circu-

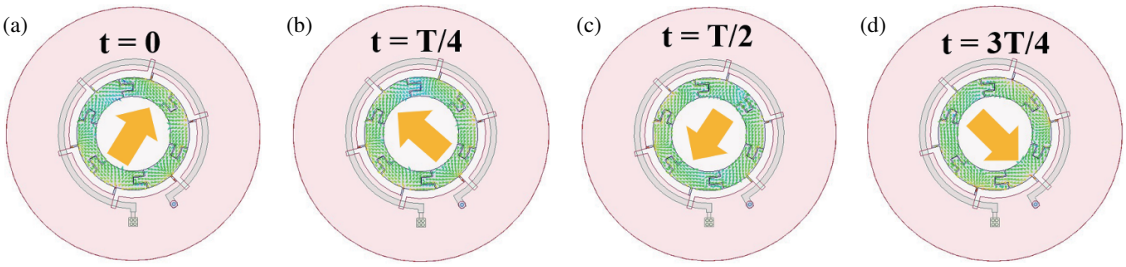

FIGURE 5. The current distribution of the antenna. (a) $t = 0$. (b) $t = T/4$. (c) $t = T/2$. (d) $t = 3T/4$.

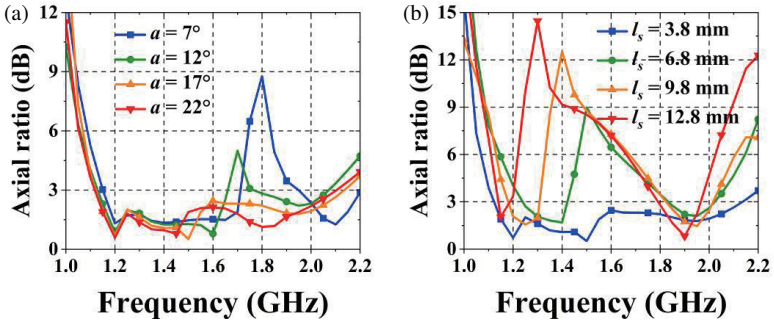

FIGURE 6. Effect of (a) a and (b) l_s on AR bandwidth.

lar polarization (RHCP) radiation. As illustrated in Figure 3, within the frequency range of 0.26 GHz to 3.04 GHz (168.4%), the $|S_{11}|$ value is less than -10 dB, while the AR bandwidth spans 1.10 GHz to 2.14 GHz (64.2%). The results demonstrate that Ant. 1 exhibits wideband feature. However, as illustrated in Figure 4, the 3-dB ARBWs at two cut planes are only 100° and 98°, respectively with the corresponding HPBWs being 87° and 90°.

In order to broaden the 3-dB ARBWs and reduce the backward radiation, a RIS was introduced beneath Ant. 1 and results in Ant. 2 (see Figure 2(b)). The RIS is placed directly below the antenna. Since the construction of traditional metal reflector necessitates the fulfilment of specific requirements ($\lambda/4$ distance), the RIS with adjustable reflective phase shift is employed as a replacement to reduce the profile. Besides, the RIS is capable of modifying the phase of wave reflection, thereby enabling the amplitude-phase relationship between two linearly polarized components in a CP antenna to be adjusted. As a result, the antenna can get wider 3-dB ARBWs. As illustrated in Figure 4, the 3-dB ARBWs at the two cut planes are widened to 146° and 116°, respectively. In addition, as seen from Figure 3(a), the introduction of RIS has little effect on matching and AR bandwidth, where the corresponding values are 153.04% (0.4 ∼ 3.05 GHz) and 60.32% (1.1 ∼ 2.05 GHz), respectively. However, the increment of 3-dB ARBW at $\varphi = 90°$ is not enough, and the HPBWs at the two cut planes are narrowed as a sacrifice (reduced to be less than 80°).

To further expand the 3-dB ARBW without affecting the HPBW, a RIS cavity is used to replace the RIS plane (named as Ant. 3), as shown in Figure 2(c). As illustrated in Figure 4, the HPBW is comparable to that of the initial antenna, with a beamwidth of both 92° at $\varphi = 0°$ and $\varphi = 90°$. In addition, the 3-dB ARBW of Ant. 3 is surprisingly extended to 232° and 214° for $\varphi = 0°$ and $\varphi = 90°$, respectively. Since the changing of reflector only affects the radiation performance, the impedance matching and AR performances remain almost unchanged, as can be seen in Figure 3.

3. PARAMETER ANALYSIS

To provide further clarification regarding the design mechanism of the proposed antenna, this section will analyze the main parameters in detail. It is noted that the remaining parameters are fixed at their final optimized values throughout the course of the analysis.

3.1. Effect of Loop Patch Slot a and Ground Slot l_s

Firstly, the loop patch slot angle a and the length of the ground slot l_s are studied. Figure 6 illustrates the AR performances varied with a and l_s. As seen in Figure 6(a), since the slot is insufficiently sized when a is 7°, the AR performance is suboptimal at high frequencies. An increase in a is accompanied by a gradual decline in the peak AR value at the higher frequency, which falls below 3 dB. It indicates that the CP performance improves, and the AR bandwidth widens. Finally, $a = 17°$ is selected considering the widest AR bandwidth.

The AR bandwidth is highly affected by length l_s. As can be seen in Figure 6(b), the AR bandwidth is obviously narrowed along with the increase of l_s. When the l_s decreases gradually to approximately 3.8 mm, the CP bandwidth of the antenna is broadened.

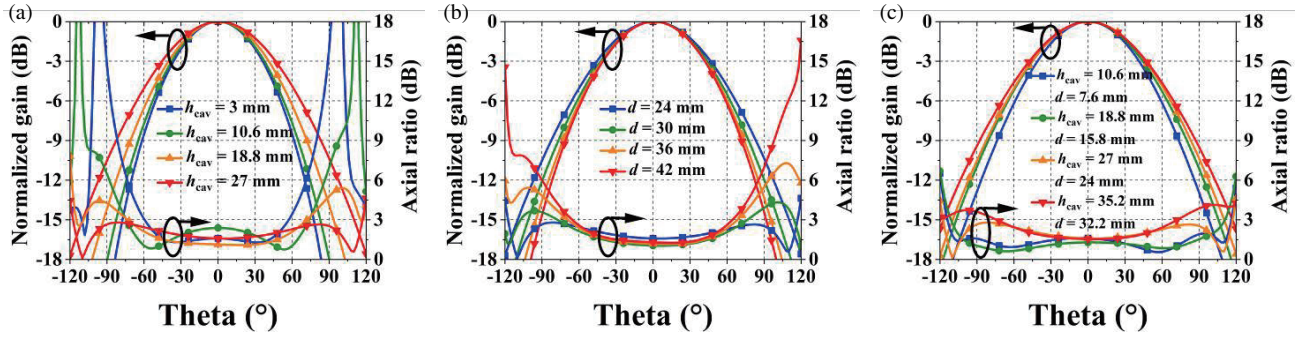

FIGURE 7. Effect of RIS cavity parameters on beamwidth. (a) h_{cav}. (b) d. (c) h_{cav} and d.

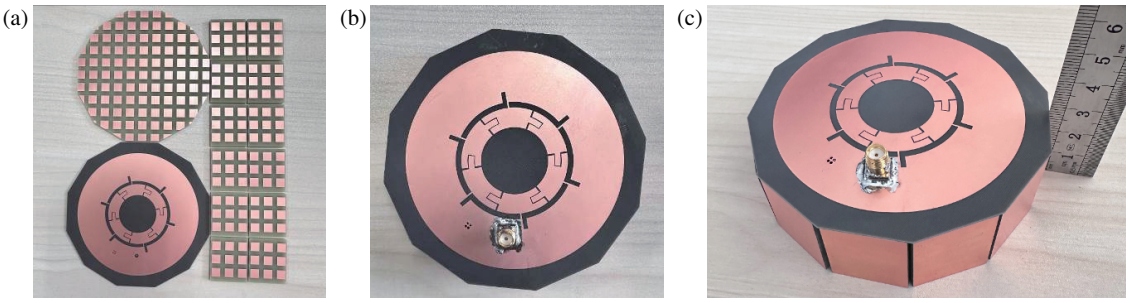

FIGURE 8. Photograph of the fabricated prototype. (a) Components. (b) Top view. (c) 3D view.

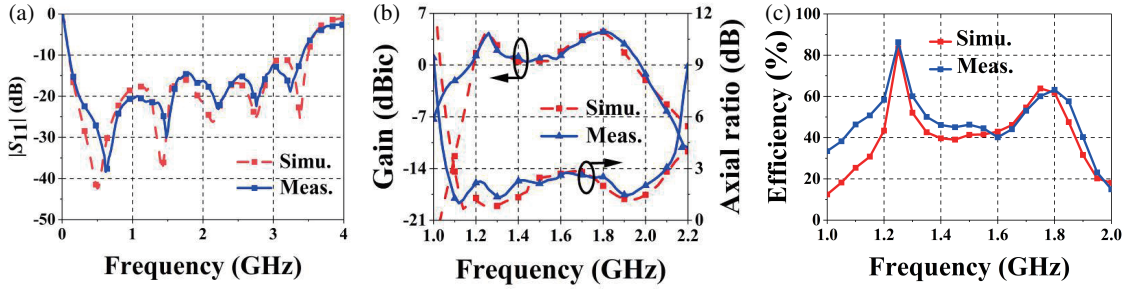

FIGURE 9. Simulated and measured results of the antenna. (a) $|S_{11}|$. (b) Gain and AR. (c) Radiation efficiency.

3.2. Effect of the RIS Cavity

Next, the parameters of the RIS cavity are analyzed, including its height (h_{cav}) and the distance (d). It is pertinent to highlight that when $d + h_2 = h_{\text{cav}}$, the cavity side wall is in contact with the loop antenna substrate. Figure 7(a) illustrates the impact of modifying the h_{cav} while maintaining a fixed d Figure 7(b), in contrast, depicts the influence of varying the d while keeping h_{cav} unaltered. Figure 7(c) illustrates that both h_{cav} and d undergo a simultaneous change, and $d + h_2 = h_{\text{cav}}$ is maintained.

It can be seen from the figure that an increase in h_{cav} is accompanied by a corresponding rise in both HPBW and 3-dB ARBW. It is noteworthy that when h_{cav} is equal to 3 mm, the configuration is that of a RIS plate rather than a RIS cavity. At this point, the HPBW is only 72°, and the 3-dB ARBW is 114°. With the increase of distance d, both HPBW and 3-dB ARBW decrease. When d is increased to 42 mm, HPBW is 80°, and 3-dB ARBW is reduced to 128°. From Figure 7(c), it can be discerned that when $h_{\text{cav}} = 35.2$ mm and $d = 32.2$ mm, the widest HPBW reaches 93°. Nevertheless, the 3-dB ARBW exhibited a declining trajectory, and its HPBW was analogous to that observed when $h_{\text{cav}} = 27$ mm and $d = 24$ mm (HPBW of this parameter was 92°). After comprehensive consideration, the parameters of $h_{\text{cav}} = 27$ mm and $d = 24$ mm were identified as the optimal choice. At this juncture, the HPBW was 92°, and the 3-dB ARBW was 232°.

4. EXPERIMENTAL RESULTS

In order to ensure the accuracy and reliability of the data, the antenna prototype is manufactured and subjected to rigorous testing. Figure 8 shows photographs of the prototype with the same parameters as in Table 1. The loop patch, ground, and feed line are printed on an F4B substrate, while the RIS cavity are printed on an FR4 substrate. In order to achieve impedance matching, it is necessary to solder a 50-ohm SMA interface and a 50-ohm resistor on both ends of the feed line.

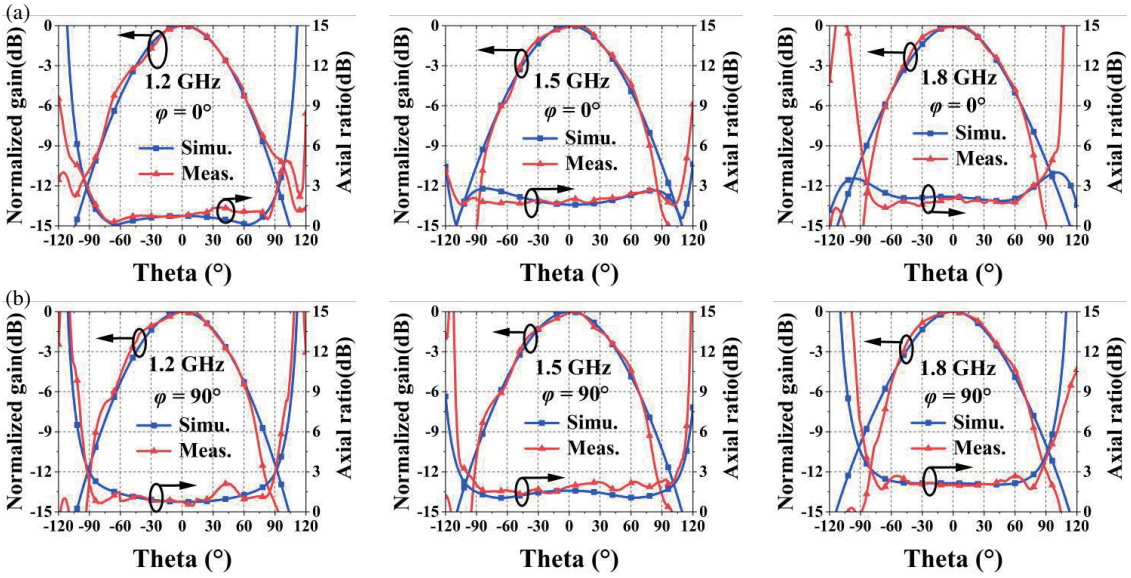

FIGURE 10. Measured and simulated ARBWs and HPBWs of the fabricated antenna at 1.2 GHz, 1.5 GHz and 1.8 GHz. (a) $\varphi = 0°$. (b) $\varphi = 90°$.

TABLE 2. Comparison of the designed antenna with other antennas.

Ref.	FBW (%)		Overlapped FBW (%)	HPBW (°)	ARBW (°)	Dimensions ($\lambda_0 \times \lambda_0 \times \lambda_0$)
	10-dB RL	3-dB AR				
[15]	39	37	37	60*	> 140	$0.48 \times 0.48 \times 0.10$
[17]	47.1	45.7	45.7	55*	203	$0.62 \times 0.62 \times 0.13$
[19]	46.3	13	13	103	202	$0.57 \times 0.57 \times 0.29$
[21]	19	16.8	16.8	130	130	$0.61 \times 0.61 \times 0.61$
[22]	62.6	42	42	82	142	$1.48 \times 1.48 \times 0.30$
[23]	55.8	70.9	55.8	96	100	$0.52 \times 0.52 \times 0.15$
[24]	92.6	71.8	71.8	120	100	$0.40 \times 0.40 \times 0.15$
This work	187.5	64.98	64.98	$90 \sim 92$	$162 \sim 224$	$0.33 \times 0.33 \times 0.10$

*Estimated from the results. λ is the wave length at the lowest operating frequency.

Figure 9 gives the simulated and measured results. The measured results are basically consistent with the simulation ones. The discrepancies between the two sets of data can be attributed to inherent inaccuracies associated with the assembly and welding processes employed in the construction of the antenna. The results shown in Figure 9(a) indicate that $|S_{11}|$ is less than -10 dB in the frequency band $0.11 \sim 3.41$ GHz, with a measured bandwidth of 187.5%. As can be seen from Figure 9(b), the 3-dB AR bandwidth is 64.98% (1.07 GHz to 2.1 GHz). Besides, the antenna exhibits a peak gain of 4.5 dBic within the frequency range of 1.17 to 1.97 GHz. Figure 9(c) gives the radiation efficiencies of the proposed antenna. From 1.1 to 1.8 GHz, simulation and measurement results indicate that the efficiency exceeds 40%. In Section 5, the reason for decreased efficiency at intermediate band is discussed.

Figure 10 illustrates the simulated and measured HPBWs and 3-dB ARBWs, with 1.2 GHz, 1.5 GHz, and 1.8 GHz selected for distribution across the frequency bands. In Figures 10(a) and (b), it can be seen that in two cutting planes $\varphi = 0°$ and $\varphi = 90°$, the measured HPBW exceeds 90° for all three frequencies, with an approximate value of $92° \pm 2°$. At $\varphi = 0°$ plane, the measured 3-dB ARBWs at 1.2 GHz, 1.5 GHz, and 1.8 GHz are 185°, 224°, and 162°, respectively. While at $\varphi = 90°$ plane, the corresponding values are 182°, 205°, and 164°, respectively. The radiation direction diagram for antenna simulation and measurement is presented in Figure 11. From the data presented in the diagram, it can be observed that the antenna exhibits effective directional radiation characteristics at both angles of all three frequencies under consideration.

Table 2 compares the performance of the proposed antenna with that of the wideband wide-beam CP antenna. For the CP antennas in [15], the feeding mode of sequential rotating traveling wave feeding is adopted like the proposed antenna. Although this feeding method results in the attainment of broadband width, the advantage is still relatively modest including the bandwidth, HPBW, and 3-dB ARBW. For [17], although wide bandwidth is achieved, only 3-dB ARBWs are improved. Insufficient bandwidth represents the most significant disad-

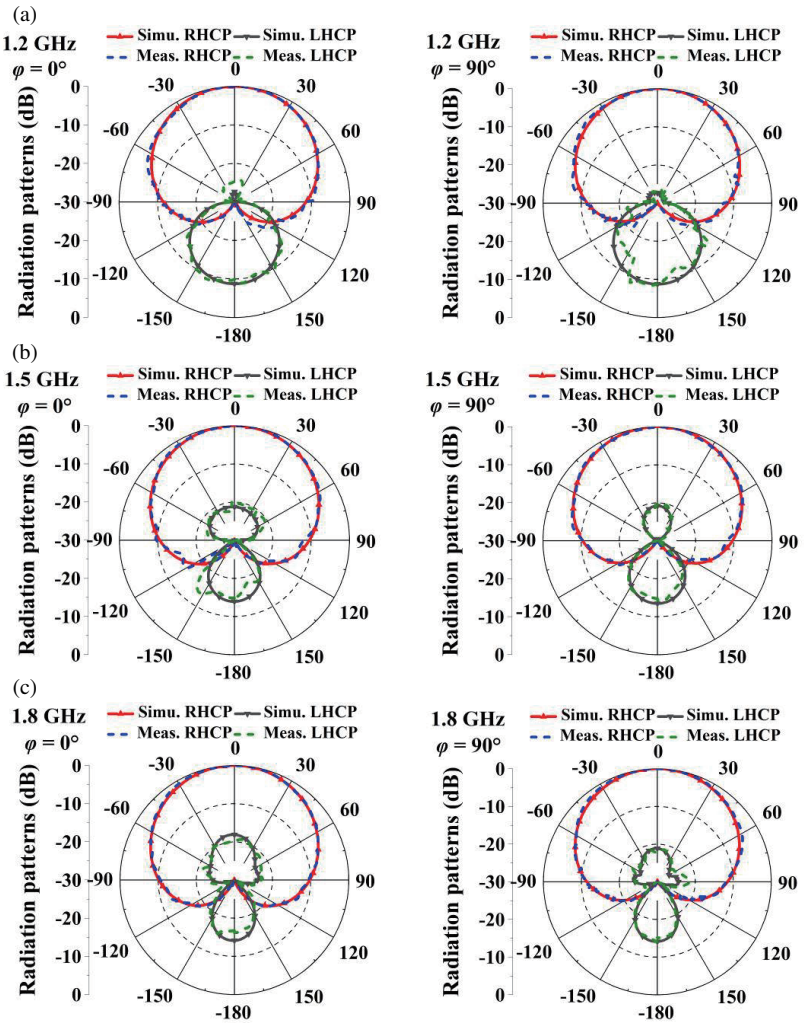

FIGURE 11. Measured and simulated radiation patterns of the fabricated antenna at $\varphi = 0°$ and $\varphi = 90°$. (a) At 1.2 GHz. (b) At 1.5 GHz. (c) At 1.8 GHz.

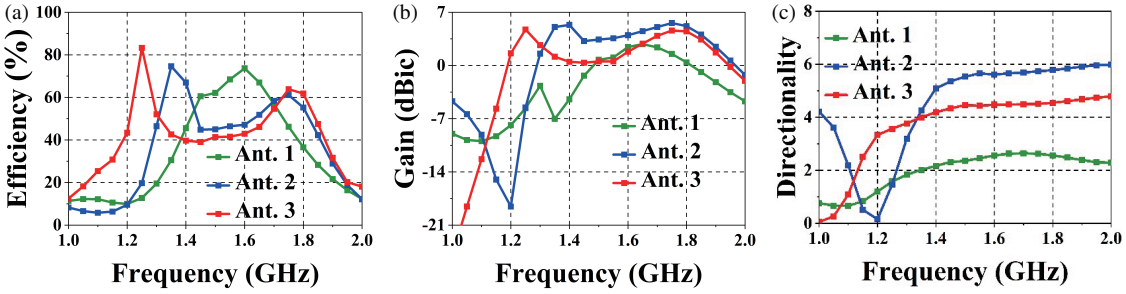

FIGURE 12. Simulated results of the three evolutions. (a) Radiation efficiency. (b) Gain. (c) Radiation directionality.

vantage associated with [19] and [21]. While a wider HPBW is achieved, the size remains excessive. For [22], the performance is satisfactory, yet the size is large. For antennas in [23] and [24], the width of 3-dB ARBW is the biggest disadvantage. In comparison, the proposed antenna exhibits wide operation bandwidth, wide 3-dB ARBW, wide HPBW, and small size, which can be a good candidate for wideband wide-beam CP applications.

5. DISCUSSION

Figure 12 shows the comparison of efficiency, gain, and directivity of the three structures of antenna evolution. Ant. 1 is a loop antenna structure, exhibiting optimal efficiency within the 1.4–1.8 GHz frequency band. However, the antenna gain is relatively modest, as illustrated in Figure 12(b). As illustrated in Figure 12(c), the antenna exhibits suboptimal directivity. This is because the antenna of this structure exhibits a considerable

backward radiation, which results in a poor directional radiation and a bidirectional radiation that is unsuitable for the actual terminal equipment. Ant. 2 introduced a RIS planar reflector, which led to a notable enhancement in the antenna's directivity. Furthermore, gains have been observed to have increased. However, as illustrated in Figure 4, a comparison reveals that the HPBW of the antenna has been reduced due to an improvement in directivity. Ant. 3 represents an extension of Ant. 2. Ant. 3 introduces a RIS sidewall, thus forming a RIS cavity. As illustrated in Figure 2, a decline in gain is observed, resulting in diminished efficiency, and the directionality is diminished, yet the HPBW of this structure is broader than Ant. 2. The observed gain loss can be attributed to partial energy loss at various frequency points resulting from the reflection phase at different positions after the reflector is introduced. By lowering the vertex gain, the HPBW is broadened as an exchange.

As widely acknowledged in the field, efficiency is the ratio of gain to directivity. The enhancement of directivity and the reduction of partial gain result in a decrease in the efficiency of some frequency bands.

6. CONCLUSION

This paper presents the design of a wideband wide-beam CP antenna, realized through the utilization of sequential rotation feeding technology. The incorporation of feeding technology and the introduction of RIS have resulted in the generation of broadband and wide-beam radiation. The results of the measurement demonstrate that the maximum 3-dB ARBW of 224° can be achieved at an operating bandwidth of 64.98% (1.07 GHz to 2.1 GHz) by loading the RIS cavity. Besides, the HPBW can be maintained above 90°. Since the antenna has wide bandwidth, wide beam and compact size, it is suitable for a multitude of application scenarios. Moreover, it can be employed as a suitable contender for Global Navigation Satellite System (GNSS) applications.

ACKNOWLEDGEMENT

This work was supported in part by the National Natural Science Foundation of China under Grant 51809030, in part by the Liaoning Revitalization Talents Program under Grant XLYC2007067, in part by the Young Elite Scientists Sponsorship Program by CAST under Grant 2022QNRC001 and in part by the Fundamental Research Funds for the Central Universities under Grant 3132024239.

REFERENCES

[1] Cheng, Y. and Y. Dong, "Wideband circularly polarized split patch antenna loaded with suspended rods," *IEEE Antennas and Wireless Propagation Letters*, Vol. 20, No. 2, 229–233, 2021.

[2] Wen, L., S. Gao, B. Sanz-Izquierdo, C. Wang, W. Hu, X. Ren, and J. Wu, "Compact and wideband crossed dipole antenna using coupling stub for circular polarization," *IEEE Transactions on Antennas and Propagation*, Vol. 70, No. 1, 27–34, 2022.

[3] Zhou, Q. L., X. Chen, and G. Fu, "A miniaturized wideband circularly polarized antenna based on tightly coupled monopole," *IEEE Antennas and Wireless Propagation Letters*, Vol. 23, No. 6, 1864–1868, 2024.

[4] Chen, Z., W. Hu, Y. Gao, L. Wen, C. Li, Z. Hu, W. Jiang, and S. Gao, "Compact wideband circularly polarized loop antenna based on dual common and differential modes," *IEEE Antennas and Wireless Propagation Letters*, Vol. 21, No. 8, 1567–1571, 2022.

[5] Wu, R., J.-H. Lin, G.-H. Wen, S.-T. Cai, and F.-C. Chen, "A compact broadband circularly polarized antenna with novel tilt fences for gnss applications," *IEEE Antennas and Wireless Propagation Letters*, Vol. 23, No. 5, 1528–1532, 2024.

[6] Zhao, Z.-B., W.-J. Lu, L. Zhu, and J. Yu, "Wideband wide beamwidth full-wavelength sectorial dipole antenna under dual-mode resonance," *IEEE Transactions on Antennas and Propagation*, Vol. 69, No. 1, 14–24, 2021.

[7] Xue, H., L. Wu, Z.-L. Xiao, and T.-Y. Hu, "A low-profile broadband circularly polarized patch antenna with wide axial-ratio beamwidth," *IEEE Antennas and Wireless Propagation Letters*, Vol. 22, No. 9, 2115–2119, 2023.

[8] Cai, X. and K. Sarabandi, "Broadband omnidirectional circularly polarized antenna with asymmetric power divider," *IEEE Transactions on Antennas and Propagation*, Vol. 68, No. 7, 5171–5181, 2020.

[9] Xu, R., Z. Shen, and S. S. Gao, "Compact-size ultra-wideband circularly polarized antenna with stable gain and radiation pattern," *IEEE Transactions on Antennas and Propagation*, Vol. 70, No. 2, 943–952, 2022.

[10] Min, C. and C. E. Free, "Analysis of traveling-wave-fed patch arrays," *IEEE Transactions on Antennas and Propagation*, Vol. 57, No. 3, 664–670, 2009.

[11] Qi, Z., Y. Zhu, and X. Li, "Compact wideband circularly polarized patch antenna array using self-sequential rotation technology," *IEEE Antennas and Wireless Propagation Letters*, Vol. 21, No. 4, 700–704, 2022.

[12] Wu, J., Z. Huang, X. Ren, W. E. I. Sha, and X. Wu, "Wideband millimeter-wave dual-mode dual circularly polarized OAM antenna using sequentially rotated feeding technique," *IEEE Antennas and Wireless Propagation Letters*, Vol. 19, No. 8, 1296–1300, 2020.

[13] Zhang, H., F. Zhang, F. Sun, Y. Heng, and J. Su, "Wideband circularly polarized applications: Design of a compact, traveling-wave-fed loop antenna," *IEEE Antennas and Propagation Magazine*, Vol. 62, No. 1, 34–39, 2020.

[14] Wu, J., W. Yang, L. Gu, Q. Xue, and W. Che, "Low-profile wideband dual-circularly polarized metasurface antenna based on traveling-wave sequential feeding mechanism," *IEEE Antennas and Wireless Propagation Letters*, Vol. 21, No. 6, 1085–1089, 2022.

[15] Zhong, Z.-P. and X. Zhang, "A travelling-wave-fed slot spiral antenna with wide axial-ratio bandwidth and beamwidth for GNSS applications," *IEEE Open Journal of Antennas and Propagation*, Vol. 2, 578–584, 2021.

[16] Liu, S., D. Yang, and J. Pan, "A low-profile circularly polarized metasurface antenna with wide axial-ratio beamwidth," *IEEE Antennas and Wireless Propagation Letters*, Vol. 18, No. 7, 1438–1442, 2019.

[17] Liu, H., J. Wang, Z. Zhao, Z. Wang, and S. Fang, "Design of wideband GNSS antenna with wide-angle circular polarization and anti-multipath performance for high precision marine positioning," *IEEE Transactions on Vehicular Technology*, Vol. 72, No. 5, 6281–6293, 2023.

[18] Sun, Y.-X., K. W. Leung, and K. Lu, "Broadbeam cross-dipole antenna for GPS applications," *IEEE Transactions on Antennas and Propagation*, Vol. 65, No. 10, 5605–5610, 2017.

[19] Sun, Y.-X., K. W. Leung, and J. Ren, "Dual-band circularly polarized antenna with wide axial ratio beamwidths for upper hemispherical coverage," *IEEE Access*, Vol. 6, 58 132–58 138, 2018.

[20] Zhong, Z.-P., X. Zhang, J.-J. Liang, C.-Z. Han, M.-L. Fan, G.-L. Huang, W. Xu, and T. Yuan, "A compact dual-band circularly polarized antenna with wide axial-ratio beamwidth for vehicle GPS satellite navigation application," *IEEE Transactions on Vehicular Technology*, Vol. 68, No. 9, 8683–8692, 2019.

[21] Xia, L.-X., N.-W. Liu, L. Zhu, and G. Fu, "Dual-CP antenna with wide-HPBW and wide-ARBW performance for wide-angle scanning phased array," *IEEE Transactions on Antennas and Propagation*, Vol. 72, No. 5, 4583–4588, 2024.

[22] Zhang, L., S. Gao, Q. Luo, P. R. Young, W. Li, and Q. Li, "Inverted-S antenna with wideband circular polarization and wide axial ratio beamwidth," *IEEE Transactions on Antennas and Propagation*, Vol. 65, No. 4, 1740–1748, 2017.

[23] Yan, Y.-D., Y.-C. Jiao, C. Zhang, Y.-X. Zhang, and G.-T. Chen, "Hemispheric conformal wide beamwidth circularly polarized antenna based on two pairs of curved orthogonal dipoles in space," *IEEE Transactions on Antennas and Propagation*, Vol. 69, No. 11, 7900–7905, 2021.

[24] Li, G. and F.-S. Zhang, "A compact broadband and wide beam circularly polarized antenna with shorted vertical plates," *IEEE Access*, Vol. 7, 90 916–90 921, 2019.